Toward a practical ultrasound waveform tomography algorithm for improving breast imaging

Cuiping Li[1,2], Gursharan Singh Sandhu[3], Olivier Roy[1,2], Neb Duric[1,4],Veerendra Allada[1], Steven Schmidt[1,2]

[1]Delphinus Medical Technologies, 46701 Commerce Center Drive, Plymouth, MI 48170; Email: cli@delphinusmt.com

[2]Department of Oncology, Wayne State University, USA,

[3]Department of Physics and Astronomy, Wayne State University, USA,

[4]Karmanos Cancer Institute, USA

ABSTRACT

Ultrasound tomography is an emerging modality for breast imaging. However, most current ultrasonic tomography imaging algorithms, historically hindered by the limited memory and processor speed of computers, are based on ray theory and assume a homogeneous background which is inaccurate for complex heterogeneous regions. Therefore, wave theory, which accounts for diffraction effects, must be used in ultrasonic imaging algorithms to properly handle the heterogeneous nature of breast tissue in order to accurately image small lesions. However, application of waveform tomography to medical imaging has been limited by extreme computational cost and convergence. By taking advantage of the computational architecture of Graphic Processing Units (GPUs), the intensive processing burden of waveform tomography can be greatly alleviated. In this study, using breast imaging methods, we implement a frequency domain waveform tomography algorithm on GPUs with the goal of producing high-accuracy and high-resolution breast images on clinically relevant time scales. We present some simulation results and assess the resolution and accuracy of our waveform tomography algorithms based on the simulation data.

Keywords: breast imaging, Graphic Processing Units, ultrasound tomography, waveform tomography

1. INTRODUCTION

Breast cancer is the second-leading cause of cancer death for American women. Early detection is the best known means for reducing cancer mortality. Ultrasound tomography imaging techniques show tremendous potential to detect and diagnosis early stage breast cancer. The idea of solving acoustic inverse problems in medicine can be traced back to the work of Wilde and Reid[1] and Howry and Bliss[2] in the 1950's. Since then, a number of investigators have developed ultrasound scanners based on the principles of ultrasound tomography.[3-9]

So far, mainly two types of ultrasound tomography algorithms are explored by different investigators. The first one is a ray-based algorithm which utilizes the eikonal equation and is thus a high frequency approximation that does not incorporate diffraction effects.[3,10] The second one either incorporates diffraction effects[11] or it utilizes full wave propagation (waveform tomography).[4,5,7] Although a ray based technique is robust and computationally cheap, it fails when diffraction effects dominate the recorded ultrasonic data. Waveform tomography models ultrasound propagation through tissue using an exact wave equation rather than a ray approximation and is capable of making images of greater accuracy and spatial resolution than previously possible. However, application of waveform tomography to medical imaging has been limited by the extreme computational cost associated with this approach as well as the convergence to local minima in the inversion process. The emergence of Graphic Processing Units (GPUs) sheds promising light on alleviating this computational burden. For real data, using the ray-based

Medical Imaging 2014: Ultrasonic Imaging and Tomography, edited by Johan G. Bosch, Marvin M. Doyley, Proc. of SPIE Vol. 9040, 90401P · © 2014 SPIE
CCC code: 1605-7422/14/$18 · doi: 10.1117/12.2043686

reconstruction as a starting model for waveform tomography is necessary to overcome convergence issues.

In this paper we will explore the feasibility of combining waveform tomography with a ring array for breast cancer imaging to achieve greater accuracy and spatial resolution than previously possible. We also speed up the computation by taking advantage of the GPU computational architecture. Analyses results and reconstruction examples are shown in Section 3.

2. MATERIALS AND METHODS

Although ultrasound waveform tomography for breast imaging is attractive in terms of accuracy and resolution, its large computational cost strongly constrains the clinical application of the method. The Delphinus Medical Technologies SoftVue system utilizes a blade server design with 8 Tesla GPUs for its standard configuration. This provides an ideal platform for realistic application of waveform tomography to clinical breast imaging. In this research, we optimize and adapt a frequency domain waveform tomography algorithm for compatibility with the SoftVue GPU blade server architecture. We assess the accuracy and resolution of the new method with numerical breast models. We also investigate the computational speed of waveform tomography for practical clinical applications.

2.1 Ultrasound waveform tomography in the space-frequency domain

Forward modeling

Forward modeling of ultrasound waveform tomography can be described by the Helmholtz equation

$$(\nabla^2 + k^2)u(\omega, c) = f(\omega), \qquad k = \frac{\omega}{c} \tag{1}$$

where k is the wavenumber, c is the velocity of the propagating media, and u is the Fourier-transformed complex-valued wavefield. Equation (1) can be represented compactly by

$$S(\omega, c)u(\omega, c) = f(\omega) \text{ or } u(\omega, c) = S(\omega, c)^{-1} f(\omega) \tag{2}$$

where $S(\omega, c)$ is the impedance matrix computed by numerical approximation of the underlying partial differential equation.[12,13] The stencil values were calculated using a 9-point 2-D scalar wave extrapolator.[14] We model absorbing boundary conditions on the boundary by forcing only inward propagating wave solutions on the boundary. Details can be found in Engquist and Majda's paper.[15]

To solve equation (2) for a multiple source problem, it is best to use direct matrix factorization methods such as LU decomposition.[16] If we use LU decomposition to solve equation (2), we can use the same matrix factors to solve for multiple sources without the need to refactor the impedance matrix S. This is critical in terms of computational cost for the iterative solution of an inverse problem with multiple sources. In this study, we utilize the highly optimized open source package $SuperLU$ to factorize the matrix S.[17,18]

Inversion algorithm

The inverse problem is to estimate a set of model parameters c from the recorded data. Assume we have n observations recorded by receivers which are evenly distributed along a 20 cm diameter ring which mimics the SoftVue transducer ring. To solve the inverse problem, we try to reduce the misfit between the observed data d_i and the modelled data $u_i(c)$ by iteratively updating the model. The modelled data $u_i(c)$ are based on the model parameter c**.** The residual error δd at the n receiver positions is defined as the difference between the modelled data and the observed data

$$\delta d_i = u_i(c) - d_i, \qquad i = 1, 2, \cdots, n \tag{3}$$

From now on, for notational simplicity, we will omit the frequency term ω. To solve the inverse problem, we try to form the cost function $E(c)$ and minimize δd in the least-square sense[1]

$$E(c) = \frac{1}{2}\delta d^t \delta d^* \tag{4}$$

We follow the gradient method to solve equation (4). Consider a parameter c

$$c^{k+1} = c^k - \alpha^k \nabla_c E^k \tag{5}$$

where k is the iteration number and α is the step length chosen by line search or approximation methods. In this study, we follow Pratt and Song's method to solve the inverse problem.[12,19] In their method, the gradient is given by

$$\nabla_p E = \frac{\partial E}{\partial p} = J^t \delta d^* = F^t v, \qquad v = [S^{-1}]\delta d^* \tag{6}$$

The matrix J is the Frechét derivative matrix, F is the virtual source term, and v is the back-propagated wavefields. For more details on how to solve the inverse problem using virtual sources, the back-propagation method, and source estimation, refer to the papers by Pratt and Song et al.[12,19]

2.2 Sound Speed and Attenuation Reconstruction

In our study, the model parameter can be represented by $c = c_R + ic_I$ which is the complex-valued velocity of the propagating media. The real part c_R is the phase velocity of the propagating media, and attenuation is introduced through the imaginary part c_I. Note that even though the velocity of the propagation medium c is a complex quantity, the cost function is a real quantity. Therefore, in order to use gradient methods to update each individual model parameters c_R or c_I, we consider the cost function to be a function of two *real* parameters c_R and c_I. We use the real part of the gradient $\nabla_{c_R} E$, the steepest descent direction, to recover the sound speed information

$${c_R}^{k+1} = {c_R}^k - \alpha^k real\left(\nabla_{c_R} E^k\right) \tag{7}$$

Likewise, to recover the attenuation information we utilize the real part of the gradient $\nabla_{c_I} E$

$${c_I}^{k+1} = {c_I}^k - \alpha^k real\left(\nabla_{c_I} E^k\right) \tag{8}$$

The attenuation is proportional to the frequency and to the inverse of the quality factor Q. The quality factor is introduced through the imaginary part c_I of the complex velocity c.[20,21]

$$\frac{1}{Q} = \frac{2k_I}{k_R} = -\frac{2c_I}{c_R} \tag{9}$$

The sound speed values of soft tissue such as the breast are in the range of $c_R = 1450 - 1550\ m/s$ and for the highest frequency used in our reconstruction 364 kHz, the quality factor chosen is about $Q = 100$ which corresponds to an attenuation of $0.065\ dB/mm$. When iteratively updating, one must choose an initial starting model based on *a priori* information. Thus, after making an initial guess, we could iterate one parameter while holding the other constant, and then do the same for the other. Likewise, we could iterate the parameters sequentially or in any other manner of our choosing. In practice, incomplete phase velocity information affects the attenuation reconstruction more drastically than how incomplete attenuation information affects the phase velocity reconstruction. This is due to the fact the scattering of the wave is introduced when there are velocity inhomogeneities. Therefore, a rough attenuation model is permissible for sound speed updates, but a more exact sound speed model is needed for attenuation updates.

2.3 Accuracy and Resolution Analyses

To analyze the resolution and accuracy of our waveform tomography algorithm, we simulated a cylindrical model consisting of a 50 mm radius 1540 m/s cylinder imbedded in a 1470 m/s background. For attenuation

reconstructions, we simulated a cylindrical model consisting of a 50 mm radius with Q = 100 imbedded in a 1540 m/s background sound speed with no attenuation. The resolution is defined by the distance of the edge response between the 10% and 90% values of the data relative to the minimum and maximum values of the reconstruction. To see the manner in which the waveform reconstruction converges to the true model as a function of iteration number, we can consider the behavior of the cost function. The accuracy is measured by the absolute value of the average residual sound speed between the reconstructed image with respect to the true model where the sum is carried over all N pixels within a chosen circular region of interest (ROI) of the reconstructed image.

$$accuracy = \left| \frac{1}{N} \sum_{i=1}^{N} (x[i]_{rec} - x[i]_{true}) \right| \tag{10}$$

2.4 Adapt to GPU Architecture

The computational expense of waveform tomography is a limiting factor in the feasibility of its use in a clinical environment. The expense can be alleviated by utilizing a Graphic Processing Unit architecture. In this study, we implement the LU triangular solver using CUSPARSE library from the Nvidia CUDA Toolkit. The computational costs of CPU implementation and GPU implementation are compared.

3. RESULTS

We have applied the described waveform tomography to simulation data and compared the reconstructed images with those of ray tomography. We further assess the resolution and accuracy of waveform tomography using cylindrical models. GPU speed-up over CPU is also analyzed.

3.1 Simulation Results of Waveform Tomography

The discussed waveform tomography algorithms were applied to a numerical breast phantom. Ten discrete frequencies from 112 KHz to 364 KHz were used for the reconstruction. Figure 1 shows the resulting sound speed image (Figure 1b), along with the true model (Figure 1a), its ray tomography counterpart (Figure 1c), and the residual of the waveform sound speed image and true model (Figure 1d).

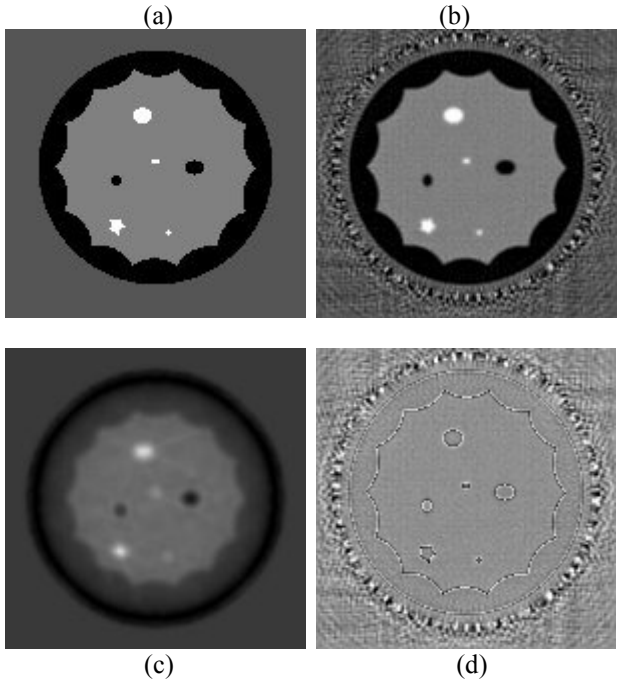

Figure 1: Sound speed reconstruction of a numerical phantom using waveform tomography. (a) True model. (b) Waveform reconstruction. (c) Ray-based reconstruction. (d) (b)-(a) residual image.

The waveform tomography nearly perfectly reconstructs the true model. The star shaped mass inclusion is well recovered (Figure 1d). The ray-based reconstruction is significantly smoother. Note that as a result of the smoothness, the five corners of the star inclusion are not well resolved.

3.2 Accuracy and Resolution Analyses

In order to quantify improvements in resolution and accuracy, we simulated a more homogeneous model consisting of a simple cylinder imbedded in a background environment. We use the average residual sound speed and the edge response of the reconstructed cylinder to measure the accuracy and resolution, respectively. Ten frequencies ranging from 112 kHz to 364 kHz were used as input to the frequency domain waveform algorithm. Five iterations were done at each frequency to update the model parameter of interest. A fine grid of $\Delta x = \Delta y = \lambda/12$ was used to create simulation data in the forward modeling process. To ensure numerical stability for lower frequencies, the number of samples per wavelength was considered for the minimum number of grid points in the model, such that the number of pixels in the horizontal direction (NX) and the number of pixels in the vertical direction (NY) both were equal to 350 pixels. During inversion, the grid size was taken to be $\Delta x = \Delta y = \lambda/10$ or $NX = NY = 300$ pixels. We compare the sound speed and attenuation reconstructions separately. For the sound speed reconstructions, we reconstructed a high sound speed disk 1540 m/s imbedded in a low sound speed background medium of 1470 m/s. No attenuation is present anywhere in the model. The starting model was homogeneous with a sound speed of 1500 m/s. For the attenuation reconstruction, we reconstructed a homogeneous sound speed model of 1540 m/s with an imbedded attenuating disk with quality factor Q = 100. The starting sound speed model was exact with a homogenous sound speed of 1540 m/s and the starting attenuation model was homogeneous with a quality factor of Q = 1000. Because higher frequencies did not improve the reconstruction, only the first five frequencies were used for the attenuation reconstruction. The ray-based reconstruction of sound speed and the waveform reconstructions of sound speed and attenuation along with true models are illustrated in Figure 2. A plot profile of the reconstructed images overlaid with the true models allows us to compare the different methods in Figure 3. The cost functions for waveform sound speed and attenuation reconstructions as a function of iteration number can be seen in Figure 4. The amount of power lost as function of quality factor can be seen in Figure 5.

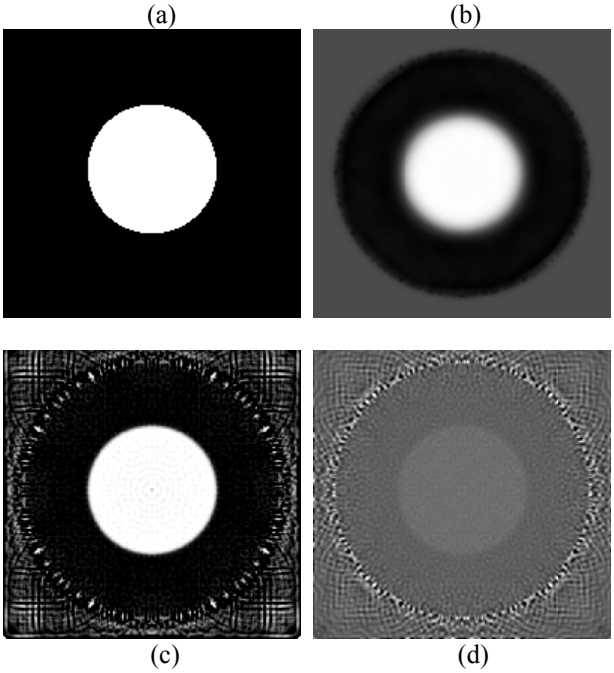

Figure 2: Sound speed and attenuation reconstructions of a numerical cylindrical phantom. (a) Sound Speed True Model (b) Ray-based sound speed (c) Waveform sound speed. (d) Waveform attenuation.

An estimate of the resolution can be given by the distance required for the edge response to rise from 10% to 90%. For the ray-based and waveform sound speed reconstructions, this corresponds to a distance of approximately 15 mm and 3 mm, respectively. The highest frequency used in the waveform reconstruction was 364 kHz, which for a background sound speed of 1500 m/s corresponds to a wavelength of 4.12 mm. The limiting resolution of the waveform method should then be approximately $\lambda/2$ = 2 mm. For a propagation distance of L = 200 mm, the limiting resolution of the ray-based reconstruction is on the order of the first Fresnel zone: $\sqrt{\lambda L}$= 14.7 mm for a dominant frequency of 1MHz. From these considerations, we see that the edge response is a fairly accurate measure of the limiting resolution in the sound speed reconstructions.

Due to its complicated nature, the attenuation reconstruction suffers from significant aliasing. Therefore, it is cumbersome to characterize its resolution in the same manner that was done for the sound speed reconstruction. We will not quote an edge response resolution, but from observing Figure 2 and 3, it can be seen that the attenuation reconstruction does have a fairly sharp interface boundary. Recovering the attenuation information is complicated because it is impossible to separate intrinsic attenuation due to tissue properties and attenuation due to velocity inhomogeneties. Taking attenuation into consideration allows for better modeling of the underlying physics and more accurate sound speed reconstructions. The attenuation properties of tissues are also clinically instructive because benign and malignant masses generally have different attenuation properties.[9]

The accuracy of the reconstructions can be assessed by considering the average residual sound speed of the reconstructed sound speed image with respect to the true model. Using an ROI with a radius of 80 mm takes the sound speed transition mismatch in to account while neglecting artifacts near the transducer ring. The ray-based and waveform reconstructions yield an average residual sound speed of 3.25 m/s and 0.24 m/s, respectively.

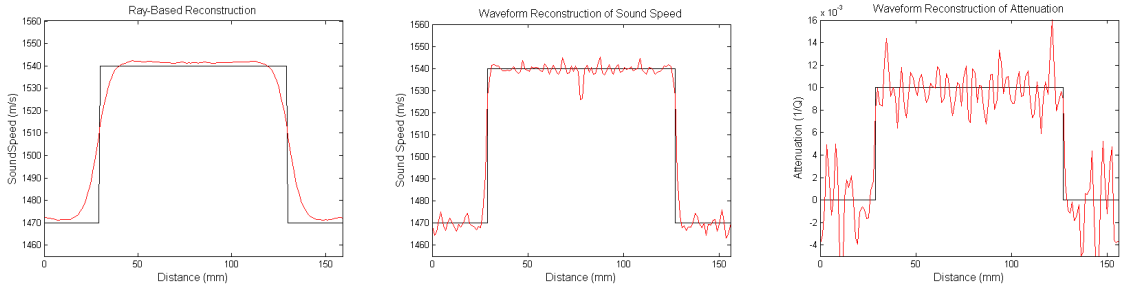

(a) (b) (c)

Figure 3: Midline profiles of sound speed and attenuation reconstructions of a numerical cylindrical phantom. (a) Ray-based sound speed. (b) Waveform sound speed. (c) Waveform attenuation.

The ray-based reconstruction is significantly smoother than the waveform reconstruction; however, the waveform reconstruction has better resolution and accuracy. The waveform reconstruction can be made smoother by damping the cost function with a regularization method such as Tikhonov regularization. For example, one could penalize perturbations δc to the previous velocity model.

$$E(c) = \frac{1}{2}\delta d^t \delta d^* + \alpha^2 \delta c^t \delta c^* \tag{11}$$

where α is the regularization parameter. The ripples in the waveform reconstruction, including the dip in the center would be reduced by such implementation. Convergence to the true model can be assessed by considering the behavior of the cost function as a function of iteration number. The cost functions of both reconstruction methods are seen in Figure 4.

Attenuation in units of 1/Q can be converted to dB/(mm Mhz) by using Figure 5. The plot was obtained by forward modeling different Q values in a completely homogeneous 1500 m/s medium with homogeneous attenuation. The field values on the aperture were then compensated for geometrical spreading. The dB loss is then given by

$$dBLoss = 20\log_{10}\left(\frac{u(\omega, Q)}{u(\omega, Q \to \infty)}\right) \tag{12}$$

The plots in Figure 5 are then given by averaging over all receivers and dividing by the average propagation distance and temporal reconstruction frequency. It can be shown[20] that the average dB loss is related to the quality factor by

$$\overline{dBLoss} = \frac{20}{\ln 10}\frac{\omega \bar{x}}{2c_R Q} \tag{13}$$

where $\bar{x}$ is the average propagation distance and $\omega = 2\pi f$. Note that in order to use Figure 5, one needs to use a the temporal frequency f as opposed to the angular frequency ω.

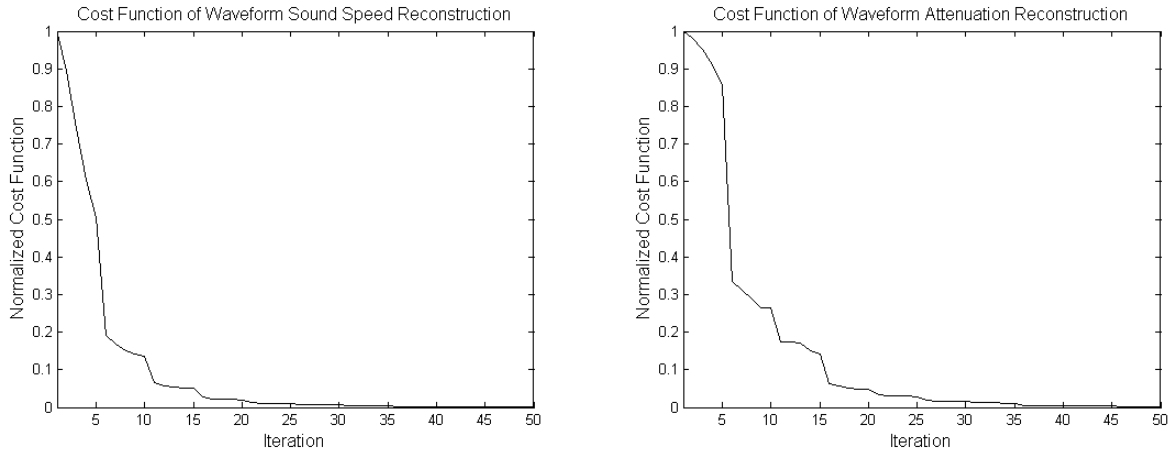

(a) (b)

Figure 4: Cost function of waveform reconstructions as a function of iteration number. (a) Sound Speed reconstruction. (b) Attenuation reconstruction.

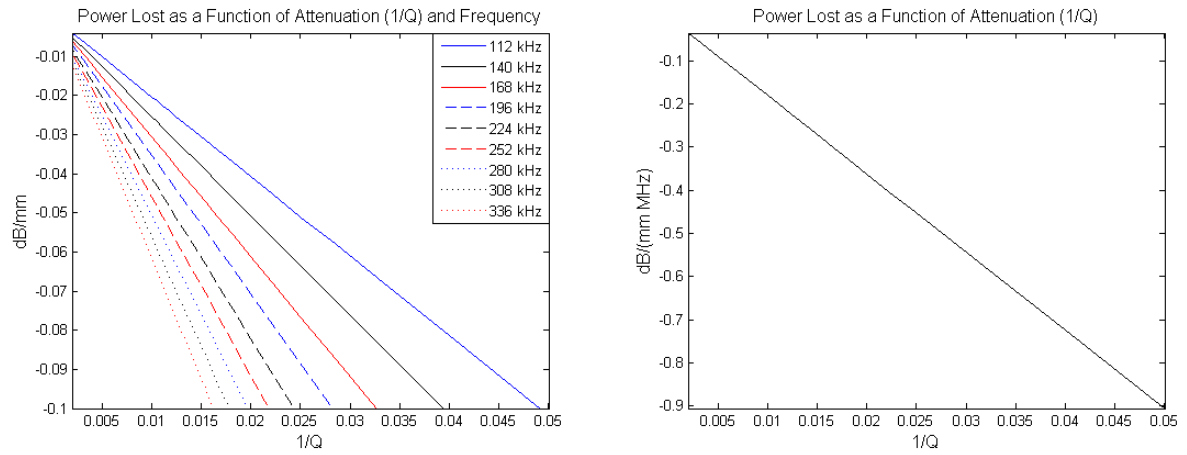

(a) (b)

Figure 5: Power lost as a function of attenuation (1/Q) and reconstruction frequency. (a) dB/mm. (b) dB/(mm Mhz).

3.3 Speed-up of GPU over CPU

Table I: GPU vs. CPU implementation cost

System to be solved (one iteration)	$Su=f$	$S^Tu=f$	Line search	Total cost
Cost of GPU implementation (seconds)	8.45	4.4	7	23.6
Cost of CPU implementation (seconds)	13.5	28.2	13.5	58.7

The computational expense of waveform tomography is a limiting factor in the feasibility of its use in a clinical environment. Some of the expense is alleviated by reconstructing in the frequency domain by choosing a discrete set of frequencies for inversion. Considering a grid size of 300 x 300 pixels, one iteration of the waveform inversion algorithm takes approximately 58.7 s without any GPU support. The computational expense is reduced to 23.6 s after we adapt the LU solver part on a Tesla C2050 GPU card. Comparison of computational cost on CPU implementation and GPU implementation is shown in Table I where $Su = f$ represents forward modeling of the normal system, $S^Tu = f$ stands for the transposed system, and line search methods are used to find the appropriate step length for model parameter update. The SoftVue blade server has 4 blades with two GPUs on each blade. We expect adapting the algorithms to the SoftVue architecture will result in more than 2x speed-up over a single GPU implementation.

4. DISCUSSION AND CONCLUSIONS

In this study, we adapt an ultrasound waveform tomography algorithm to GPU computational architecture. We assess the accuracy and resolution of the new imaging algorithms and investigate its computational speed for practical clinical applications using numerical breast models. We also show the potential resolution and accuracy improvements of the new method from the previous ray-based method.

As shown in Figure 1, waveform tomography, with only a few very low frequencies, can reconstruct the numerical breast phantom with significant advantages over ray tomography. The star shaped inclusion is well recovered in the waveform image, while in the ray-based image, all five corners are blurred out. The residual image (Figure 1d) demonstrates that waveform tomography not only recovers the edges of all inclusions (high resolution), but it also accurately recovers their sound speeds.

Further quantitative analyses of resolution and accuracy (Figure 3) reveal that the resolution of waveform tomography is about one wavelength of the highest frequency used in the reconstruction. The cost function in Figure 4 shows that the algorithm converges to a global minimum as iterations increase. The average residual sound speed error of waveform reconstruction is much smaller than that of ray-based reconstruction. As shown in Figure 3b and 3c, waveform reconstructions produce several ripples at the anomaly location. These small ups and downs can be reduced by applying regularization. The larger ripples in attenuation reconstruction (Figure 3c) are mainly due to the wave scattering caused by the sound speed inheterogeneity. Attenuation reconstruction with Tikhnov regularization for the same model as in Figure 2 is shown in Figure 6 where the ripples were reduced by adding the regularization term.

The proposed waveform tomography algorithm has been adapted to a single GPU architecture, which achieves a 2.5 factor of speed-up for a complete iteration. For the part that solves the transposed system, the GPU implementation is more than 4 times faster than CPU implementation. The same algorithm will be further optimized on our SoftVue GPU blade server that has 4 blades with two GPUs one each of the blades. We expect more than two fold further speed-up.

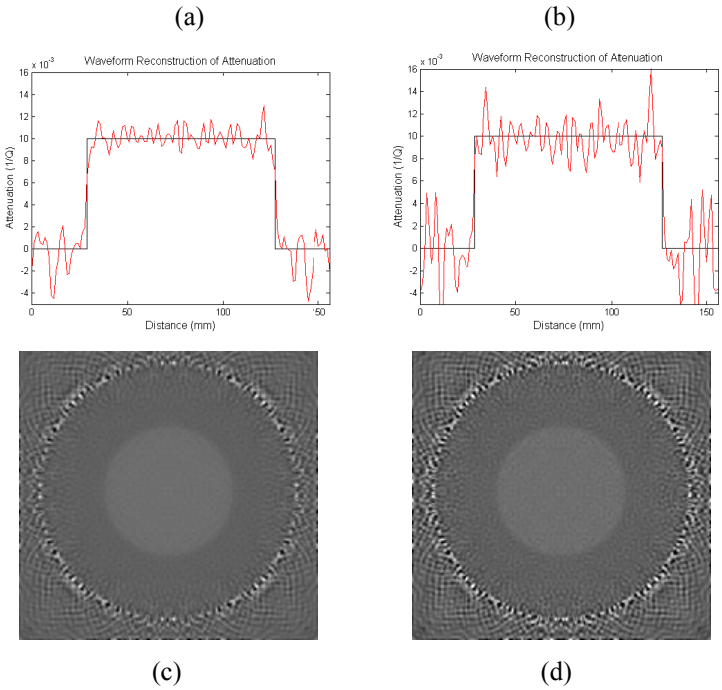

Figure 6: Midline profile and reconstructions of regularized and normal attenuation images. (a) With regularized. (b) Without regularization. (c) With regularized. (d) Without regularization.

In our simulations we use a few very low frequencies for the reconstruction. Consequently, we can use coarse grid models whose computational cost is relatively cheap. To achieve clinically relevant resolution for breast imaging we may need to go to higher frequencies that are more computationally demanding. Therefore, in order to make it clinically practical to meet patient throughput, we need to further speed up the proposed algorithm. To achieve this goal we need to investigate strategies other than GPU implementation. These include using fewer sources, conjugate gradient methods, and approximation methods for the step length. However, with our GPU implementation in place, the evolution of GPUs over time will naturally lead to commensurate decreases in the processing time leading to rapid convergence to clinical time scales.

Our simulation results are motivating and suggest that waveform tomography can substantially improve image quality. Furthermore, with implementation on GPU blade servers, it is now possible to place waveform tomography on a path to clinical relevance.

ACKNOWLEDGEMENTS

The authors acknowledge the support of the National Cancer Institute through grant 1R43CA171601-01.

REFERENCES:

1. J. J. Wild and J. M. Reid, “Application of echo-ranging techniques to the determination of structure of biological tissues,” Science 115, 226-230, 1952.
2. D. H. Howry and W. R. Bliss, “Ultrasonic visualization of soft tissue structures of the body,” J. Lab. Clin. Med., 40, 579-592, 1952.
3. P. L. Carson, C. R. Meyer, A. L. Scherzinger and T. V. Oughton, “breast imaging in coronal planes with simultaneous pulse echo and transmission ultrasound,” Science, 214, 1141-1143, 1981.
4. M. P. Andre, H. S. Janee, P. J. Martin, G. P. Otto, B. A. Spivey and D. A. Palmer, “High-speed data acquisition in a diffraction tomography system employing large-scale toroidal arrays,” International Journal of Imaging

Systems and Technology, 8, 137-147, 1997.

5. S. A. Johnson, D. T. Borup, J. W. Wiskin, F. Natterer, F. Wuebbling, Y. Zhang and C. Olsen, "Apparatus and Method for Imaging with Wavefields using Inverse Scattering Techniques," United States Patent 6,005,916, 1999.
6. V. Z Marmarelis, T. Kim and R. E. Shehada, Proceeding of SPIE: Medical Imaging; Ultrasonic Imaging and Signal Processing 2003, Paper 5035-6, 2003.
7. D-L Liu and R. C. Waag, "Propagation and backpropagation for ultrasonic wavefront design," IEEE Trans. On Ultras. Ferro. And Freq. Contr., 44, 1-13, 1997.
8. H. Gemmeke and N. Ruiter, "3D ultrasonid computer tomography for medical imaging," Nuclear instruments and methods in Physics Research SectionA: Accelerators, Spectrometers, Detectors and Associated Equipment, 580, 1057-1065, 2007.
9. N. Duric, P. Littrup, L. Poulo, A. Babkin, R. Pevzner, E. Holsapple, O. Rama and C. Glide, "Detection of Breast Cancer with Ultrasound Tomography: First Results with the Computerized Ultrasound Risk Evaluation (C.U.R.E.) Prototype," Medical Physics, 34, 773-785, 2007.
10. C. Li, N. Duric, P. Littrup and L. Huang, "In Vivo Breast sound-speed imaging with ultrasound tomography,", Ultrasound. Med. Biol., 35, 1615-1628, 2009.
11. P. Huthwaite and F. Simonetti, "High-resolution imaging without iteration: A fast and robust method for breast ultrasound tomography," J. Accoust. Soc. Am., 130, 1721-1734, 2011.
12. R. G. Pratt, "Seismic waveform inversionint he frequency domain, Part 1: Theory and verification in a physical sale model," Geophysics, 64, 888-901, 1999.
13. R. G. Pratt, L. Huang, N. Duric, N and P. Littrup, "Sound-speed and attenuation imaging of breast tissue using waveform tomography of transmission ultrasound data," in Medical Imaging 2007: Physics of Medical Imaging, Hsieh, J., Flynn, M.J., Eds., Proceedings of the SPIE, *6510*, 65104S, 2007.
14. C-H. Jo, C. Shin, and J. H. Suh, "An optimal 9-point, finite-difference, frequency-space, 2-D scalar wave extrapolator," Geophysics, Vol 61, No 2, pp. 529-537, 1996.
15. B. Engquist and A. Majda, "Absorbing Boundary Conditions for the Numerical Simulation of Waves," Mathematics of Computation, 31, 629-651, 1977.
16. R. G. Pratt, "Frequency-domain elastic wave modeling by finite differences: A tool for crosshole seismic imaging," Geophysics, 55, 626-632, 1990.
17. J. W. Demmel, S. C. Eisenstat, J. R. Gilbert, X. S. Li and J. W. H. Liu, "A SUPERNODAL APPROACH TO SPARSE PARTIAL PIVOTING," SIAM J. Matrix Anal. Appl., 20, 720-755, 1999.
18. X. S. Li, J. W. Demmel, J. R. Gilbert, L. Grigori and M. Shao, SuperLU Users; Guide, 1999.
19. Z. M. Song, P. R. Williamson and R. G. Pratt, "Frequency-domain acoustic-wave modeling and inversion of crosshole data: Part II-Inversion method, systhetic experiments and real-data results," Geophysics, 60, 796-809, 1995.
20. K. Aki and P. G. Richards, "Quantitative Seismology," second edition, edited by J. Ellis, pp. 162-163, University Science Books, printed in United States, 2009.
21. G. Nolet, "Seismic wave propagation and seismic tomography," Seismic Tomography, edited by G. Nolet, pp. 1-23, D. Reidel, Norwell, Mass, 1987.